Optimal Open-Loop Control Policies for a Class of Nonlinear Actuators

Edgar Ramirez-Laboreo, Eduardo Moya-Lasheras and Carlos Sagues

***Abstract*— This paper deals with the design and analysis of open-loop soft-landing control policies for a class of nonlinear actuators. A third-order nonlinear parametric model is firstly presented and the particularities of the systems under study are highlighted. Then, time-optimal and energy-optimal trajectories are analytically derived by means of the Pontryagin principle. Numerical solutions are obtained for a nominal model and the robustness of the obtained open-loop input profiles on perturbed systems is studied via Monte Carlo simulations. The results show that the impact velocities are efficiently reduced with any of the proposed strategies and, consequently, that open-loop control could be a practical and cost-effective approach for improving the performance of these actuators.**

I. INTRODUCTION

Electromagnetic reluctance actuators are a class of nonlinear systems which are being increasingly used because of their force density, fast response and reduced cost [1]. These actuators can be found, e.g., in vehicles [2] or in aeronautical applications [3]. In contrast to Lorentz actuators, which are driven by a force which is proportional to the coil current, the motion in reluctance actuators is related to a change in the magnetic energy stored in the system. As a consequence, the force producing the motion is nonlinear and highly dependent on the position of the mover. The behavior of this force, which is higher the smaller the air gap, together with the absence of any type of control, causes these actuators to suffer from severe impacts and wear in each operation.

In this regard, several modeling, estimation and control papers can be found in the literature dealing with the aforementioned problems. Starting with the early works of the 1960s [4], many different approaches have been adopted to analyze the dynamics and improve the performance of reluctance actuators. Dynamic modeling, for instance, has been faced via analytical [5], numerical [6] and combined [7], [8] methods, but all the models lead to similar conclusions: reluctance actuators are high-speed systems with rich and complex dynamics. Many other works have focused on finding control strategies to achieve-soft landing, i.e., controllers that force the actuator to reach the final position with zero velocity [9]. Given that the mover position cannot be measured in practice—at least not with affordable sensors—some of the solutions rely on estimations [10], [11], [12] to perform the designed control policy. However, the estimation models are usually too complex to be implemented in real time or neglect some electromagnetic phenomena, like hysteresis or eddy currents, which have a strong influence on the dynamic behavior of the device [13]. A practical approach to increase the robustness of these solutions is the use of cycle-to-cycle learning-type strategies that adjust the feedback controller [14] or the feedforward signal [15], [16].

Designing a feasible trajectory considering input constraints is one of the key aspects to achieve soft landing. In this connection, some previous works have applied optimal control theory to find feasible [17], time-optimal [18] or energy-optimal solutions [19]. However, disturbances or modeling errors are commonly neglected in the solutions and, therefore, the generated input profiles do not result in soft landing when applied in open loop to the actual device. Despite that, the high speed nonlinear dynamics of reluctance actuators, as well as the difficulty in measuring or estimating interest variables, motivates the search of open-loop control policies which can be easily implemented in practice. For these reasons, in this paper we present and compare five different optimal control policies to achieve soft landing on reluctance actuators. The main contribution of the work is an analysis of the open-loop application of these strategies on perturbed systems, i.e., systems which are different from the nominal model used to design the controller. This analysis is carried out via Monte Carlo simulations. The obtained results show that the impact velocities are efficiently reduced with any of the presented policies and, consequently, that open-loop control could be a practical and cost-effective approach to increase the service life of this type of actuators.

II. SYSTEM DYNAMICS

Reluctance actuators are electromechanical devices where the force that produces the motion is due to a change in the magnetic energy of the system. In particular, single-coil reluctance actuators have a coil wrapped around an iron core with a fixed and a moving part. When the coil is energized, a magnetic flux is generated, flowing through both the iron and the air gap between the stator and the mover. This produces a magnetic force which pulls the mover towards the stator and closes the gap, an operation which is usually called *making*. The opposite motion, which is commonly known as *breaking*, is driven by the elastic force produced by a spring which generally cannot be controlled. Fig. 1 schematically depicts a plunger-type reluctance actuator.

The dynamics of these actuators are governed by three basic equations. First, the electrical equation of the coil,

$$u = R\,i + N\dot{\phi}, \tag{1}$$

This work was supported in part by the Ministerio de Ciencia, Innovación y Universidades, Gobierno de España - European Union under project RTC-2017-5965-6, in part by the Ministerio de Educación, Cultura y Deporte, Gobierno de España under grant FPU14/04171, in part by DGA Scholarship Orden IIU/1/2017, and in part by project DGA-T45_17R/FSE.

The authors are with the Departamento de Informatica e Ingenieria de Sistemas (DIIS) and the Instituto de Investigacion en Ingenieria de Aragon (I3A), Universidad de Zaragoza, Zaragoza 50018, Spain (e-mail: ramirlab@unizar.es, emoya@unizar.es, csagues@unizar.es)

where u is the voltage across the terminals, R is the resistance, i is the current, N is the number of turns of the coil and ϕ is the magnetic flux. Secondly, a relation between the current and the magnetic flux, which is usually provided by Hopkinson's law [20]

$$Ni = \phi\,\mathcal{R}(z,\phi), \tag{2}$$

where $\mathcal{R}(z,\phi)$ is the reluctance of the magnetic circuit and z is the position of the actuator. Considering the great number of reluctance models in the literature [7], this variable is considered as an arbitrary function of z and ϕ. Finally, the motion dynamics is governed by Newton's second law,

$$m\,\ddot{z} = -k_{\mathrm{s}}(z - z_{\mathrm{s}}) - c\,\dot{z} + F_{\mathrm{mag}}(z,\phi), \tag{3}$$

where m is the moving mass, k_{s} is the spring stiffness, z_{s} is the actuator position at the spring equilibrium length, c is the damping coefficient (often assumed zero) and F_{mag} is the magnetic force, given by [21, p. 151]

$$F_{\mathrm{mag}}(z,\phi) = -\frac{1}{2}\,\phi^2\,\frac{\partial \mathcal{R}(z,\phi)}{\partial z}. \tag{4}$$

Then, selecting the position, the velocity and the magnetic flux as state variables,

$$\mathbf{x} = \begin{bmatrix} x_1 & x_2 & x_3 \end{bmatrix}^{\mathsf{T}} = \begin{bmatrix} z & \dot{z} & \phi \end{bmatrix}^{\mathsf{T}}, \tag{5}$$

the following state-space representation of the system is obtained

$$\dot{\mathbf{x}} = \mathbf{f}(\mathbf{x},u) = \begin{bmatrix} f_1(\mathbf{x}) & f_2(\mathbf{x}) & f_3(\mathbf{x},u) \end{bmatrix}^{\mathsf{T}}, \tag{6}$$

where the voltage u is the model input and

$$f_1(\mathbf{x}) = x_2, \tag{7}$$

$$f_2(\mathbf{x}) = \frac{1}{m}\big(F_{\mathrm{mag}}\,(x_1,x_3) - k_{\mathrm{s}}\,(x_1 - z_{\mathrm{s}}) - c\,x_2\big), \tag{8}$$

$$f_3(\mathbf{x},u) = \frac{u}{N} - \frac{R\,x_3\,\mathcal{R}(x_1,x_3)}{N^2}. \tag{9}$$

Except for some particular reluctance models that consider magnetic hysteresis [13], generally it can be assumed that

$$\mathcal{R}(z,\phi) = \mathcal{R}(z,-\phi) > 0, \tag{10}$$

which implies that $F_{\mathrm{mag}}(z,\phi) = F_{\mathrm{mag}}(z,-\phi)$, i.e., that the sign of the magnetic force does not depend on the sign of the flux. Thus, although (9) indicates that the flux may increase or decrease according to u, the magnetic force for a particular position always acts in the same direction, which clearly limits the control possibilities. Furthermore, the condition in (10) implies also that

$$f_1\left(\begin{bmatrix} z & \dot{z} & -\phi \end{bmatrix}^{\mathsf{T}}\right) = f_1\left(\begin{bmatrix} z & \dot{z} & \phi \end{bmatrix}^{\mathsf{T}}\right), \tag{11}$$

$$f_2\left(\begin{bmatrix} z & \dot{z} & -\phi \end{bmatrix}^{\mathsf{T}}\right) = f_2\left(\begin{bmatrix} z & \dot{z} & \phi \end{bmatrix}^{\mathsf{T}}\right), \tag{12}$$

$$f_3\left(\begin{bmatrix} z & \dot{z} & -\phi \end{bmatrix}^{\mathsf{T}}, -u\right) = -f_3\left(\begin{bmatrix} z & \dot{z} & \phi \end{bmatrix}^{\mathsf{T}}, u\right). \tag{13}$$

These equations show that given $u(t) = f_u(t)$ and $\phi(t_0) = \phi_0$, where t_0 is an arbitrary time, identical position and velocity trajectories would be obtained for all $t \geq t_0$ if $u(t) = -f_u(t)$ and $\phi(t_0) = -\phi_0$.

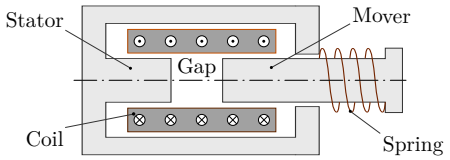

Fig. 1. Schematic representation of a plunger-type reluctance actuator.

III. OPTIMAL TRAJECTORY DESIGN

The soft-landing strategies presented in this paper are specifically designed for actuators whose position is bounded between two values $z_{\min}$ and $z_{\max}$, where $z_{\min} < z_{\max}$. In this section, the model (7)–(9) is used to derive optimal soft-landing trajectories from $z_{\min}$ to $z_{\max}$ and vice versa.

A. Problem Formulation and Solution Method

The problem of finding a bounded time-dependent input $u(t)$ which achieves a soft-landing trajectory for the actuator is formulated as follows:

$$\min_{u(t)} \quad J = \int_{t_0}^{t_{\mathrm{f}}} V\big(\mathbf{x}(t),u(t)\big)\,\mathrm{d}t, \tag{14}$$

$$\text{s. t.} \quad \dot{\mathbf{x}}(t) = \mathbf{f}\big(\mathbf{x}(t),u(t)\big), \tag{15}$$

$$\alpha \leq u(t) \leq \beta, \tag{16}$$

$$\phi(t) \geq 0 \tag{17}$$

$$\mathbf{x}(t_0) = \mathbf{x_0} = \begin{bmatrix} z_0 & 0 & \phi_0 \end{bmatrix}^{\mathsf{T}}, \tag{18}$$

$$\mathbf{x}(t_{\mathrm{f}}) = \mathbf{x_f} = \begin{bmatrix} z_{\mathrm{f}} & 0 & \phi_{\mathrm{f}} \end{bmatrix}^{\mathsf{T}}, \tag{19}$$

where J is the performance index, t_0 and t_{f} are the initial and final times, V is a scalar function, α and β are the lower and upper bounds of u and $\mathbf{x_0}$ and $\mathbf{x_f}$ are the initial and final states, respectively. It is assumed that $\alpha < 0 < \beta$.

The trajectory must start at the initial position, $x_1(t_0) = z_0$, at rest, $x_2(t_0) = 0$. Considering the system under study, z_0 corresponds to either $z_{\min}$ (breaking operation) or $z_{\max}$ (making operation). The takeoff occurs when the net force is equal to zero,

$$f_2\left(\begin{bmatrix} z_0 & 0 & \phi_0 \end{bmatrix}^{\mathsf{T}}\right) = 0, \tag{20}$$

which results in a condition for the initial flux ϕ_0. At the end of the motion, the actuator must reach the final position, $x_1(t_{\mathrm{f}}) = z_{\mathrm{f}}$, which is either $z_{\max}$ (breaking operation) or $z_{\min}$ (making operation), with zero velocity, $x_2(t_{\mathrm{f}}) = 0$. Additionally, in order to maintain that position, the final acceleration must also be set equal to zero,

$$f_2\left(\begin{bmatrix} z_{\mathrm{f}} & 0 & \phi_{\mathrm{f}} \end{bmatrix}^{\mathsf{T}}\right) = 0, \tag{21}$$

which provides the condition for the final flux ϕ_{f}.

A solution of the problem (14)–(19) can be found by following the Pontryagin method. In this regard, it should be noted that (17) is not explicitly handled in the procedure; it is simply used to rule out redundand solutions with the same mechanical trajectories (see the previous section). The optimal input is obtained by building the Hamiltonian

$$\mathcal{H}\,(\mathbf{x},\boldsymbol{\lambda},u) = V(\mathbf{x},u) + \boldsymbol{\lambda}^{\mathsf{T}}\,\mathbf{f}(\mathbf{x},u), \tag{22}$$

where $\boldsymbol{\lambda} = [\,\lambda_1\ \lambda_2\ \lambda_3\,]^{\mathsf{T}}$ is the costate, and then applying the Pontryagin principle,

$$\mathcal{H}\left(\mathbf{x}^*, \boldsymbol{\lambda}^*, u^*\right) \leq \mathcal{H}\left(\mathbf{x}^*, \boldsymbol{\lambda}^*, u\right) \quad \forall u \in [\alpha, \beta]\,, \tag{23}$$

where $\mathbf{x}^*$, $\boldsymbol{\lambda}^*$ and u^* are the optimal state, costate and input, respectively. This step results in the input expressed as a function of the state and the costate.

$$u^* = h(\mathbf{x}^*, \boldsymbol{\lambda}^*) \tag{24}$$

The dynamics of the Hamiltonian system are subsequently obtained as

$$\dot{\mathbf{x}}^*(t) = +\frac{\partial \mathcal{H}^*}{\partial \boldsymbol{\lambda}^*}, \qquad \dot{\boldsymbol{\lambda}}^*(t) = -\frac{\partial \mathcal{H}^*}{\partial \mathbf{x}^*}, \tag{25}$$

where $\mathcal{H}^* = \mathcal{H}\big(\mathbf{x}^*, \boldsymbol{\lambda}^*, h\left(\mathbf{x}^*, \boldsymbol{\lambda}^*\right)\big)$, and the trajectory is numerically computed using (18) and (19) as boundary conditions. Finally, the optimal open-loop policy is obtained by replacing $\mathbf{x}^*$ and $\boldsymbol{\lambda}^*$ in (24) by their numerical values.

B. Time-Optimal Policy

The time-optimal control policy is the one that minimizes the time taken by the actuator to go from $\mathbf{x_0}$ to $\mathbf{x_f}$. In order to find such solution, the function V is selected as

$$V(\mathbf{x}, u) = 1, \tag{26}$$

which results in $J = t_\mathrm{f} - t_0$ and in the Hamiltonian

$$\mathcal{H}\left(\mathbf{x}, \boldsymbol{\lambda}, u\right) = 1 + \lambda_1\, f_1(\mathbf{x}) + \lambda_2\, f_2(\mathbf{x}) + \lambda_3\, f_3(\mathbf{x}, u)\,. \tag{27}$$

Using (7)–(9) to apply the Pontryagin principle leads to

$$\lambda_3^*\, u^* \leq \lambda_3^*\, u \quad \forall u \in [\alpha, \beta]\,, \tag{28}$$

which allows for obtaining h as a piecewise function of λ_3^*.

$$h(\mathbf{x}^*, \boldsymbol{\lambda}^*) = \underset{u \in [\alpha, \beta]}{\operatorname{argmin}} \left(\lambda_3^*\, u\right) = \begin{cases} \beta & \text{if} \quad \lambda_3^* < 0 \\ \alpha & \text{if} \quad \lambda_3^* > 0 \end{cases} \tag{29}$$

Note however that h is not defined for $\lambda_3^* = 0$, which suggests that the time-optimal control problem is singular. This can be easily avoided by redefining V as

$$V(\mathbf{x}, u) = 1 + \epsilon\, u^2, \tag{30}$$

where $\epsilon > 0$ is an infinitely small number. Then, applying the Pontryagin principle with the regularized version of V leads to

$$h(\mathbf{x}^*, \boldsymbol{\lambda}^*) = \underset{u \in [\alpha, \beta]}{\operatorname{argmin}} \big(\epsilon\, u^2 + \lambda_3^*\, u\big) = \begin{cases} \beta & \text{if} \quad \lambda_3^* < 0 \\ 0 & \text{if} \quad \lambda_3^* = 0 \\ \alpha & \text{if} \quad \lambda_3^* > 0 \end{cases} \tag{31}$$

which is defined for all values of λ_3^* and, consequently, will not lead to singularity intervals.

Since t_f is free (it is the variable to minimize) an additional boundary condition is needed to solve the problem. The necessary conditions for optimality obtained from the classical theory of the calculus of variations [22, p. 65] [23, p. 188] provide such extra condition as

$$\mathcal{H}\Big(\mathbf{x}^*(t_\mathrm{f}), \boldsymbol{\lambda}^*(t_\mathrm{f}), h\big(\mathbf{x}^*(t_\mathrm{f}), \boldsymbol{\lambda}^*(t_\mathrm{f})\big)\Big) = 0. \tag{32}$$

C. Energy-Optimal Policy

The time-optimal solution determines the minimum amount of time required by the system to follow a soft-landing trajectory. Trajectories lasting longer than that limit can be obtained, e.g., by solving an energy-optimal problem. For that, the function V is selected as

$$V(\mathbf{x}, u) = u^2, \tag{33}$$

which results in the Hamiltonian

$$\mathcal{H}(\mathbf{x}, \boldsymbol{\lambda}, u) = u^2 + \lambda_1\, f_1(\mathbf{x}) + \lambda_2\, f_2(\mathbf{x}) + \lambda_3\, f_3(\mathbf{x}, u)\,. \tag{34}$$

In this case, the Pontryagin principle states that

$$u^{*2} + \lambda_3^*\, u^*/N \leq u^2 + \lambda_3^*\, u/N \quad \forall u \in [\alpha, \beta] \tag{35}$$

and, consequently, the energy-optimal policy h is given by

$$h(\mathbf{x}^*, \boldsymbol{\lambda}^*) = \underset{u \in [\alpha, \beta]}{\operatorname{argmin}} \left(u^2 + \lambda_3^*\, u/N\right) = \\ = \begin{cases} \beta & \text{if} \quad \lambda_3^* < -2N\beta \\ -\dfrac{\lambda_3^*}{2N} & \text{if} \quad -2N\beta \leq \lambda_3^* \leq -2N\alpha \\ \alpha & \text{if} \quad \lambda_3^* > -2N\alpha \end{cases} \tag{36}$$

which is defined for all values of λ_3^*.

IV. SIMULATION AND RESULTS

In this section, we present and compare different soft-landing optimal solutions for the making and breaking operations of a particular reluctance actuator model. The simulated dynamic model assumes a reluctance of the form

$$\mathcal{R}(z, \phi) = k_1\, z + \frac{k_2}{1 - |\phi|\,/k_3}, \tag{37}$$

where k_1, k_2 and k_3 are constants. This reluctance results from the sum of an air component which is proportional to the gap length and an iron component that includes magnetic saturation by means of the Fröhlich-Kennelly model [5].

In order to analyze the effects of the position boundaries, the control policies are evaluated using the hybrid model presented in Fig. 2. In this figure, each transition is described by its guard condition (in green) and its reset function (in red), respectively before and after a right arrow ($\Rightarrow$). The superscript $+$ is used to specify the values of the states after the jump. The reset function is explicitly shown only for those variables that change during the jump; if the transition does not imply a jump, only the guard condition is presented. The model operates as follows. If the mover is in motion and reaches any of the position boundaries, the automaton jumps to the corresponding non-motion dynamic mode and the velocity is reset to zero. Then, when the acceleration given by (8) would produce motion away from the bounds, the automaton gets back to the motion mode. For simplicity, the collisions are assumed perfectly inelastic, i.e., all the kinetic energy is dissipated at impacts. Note however that bounces will still exist when the impact velocity and the sum of the magnetic and spring forces at that moment have opposite signs. The nominal values of the parameters are presented in Table I. The voltage is bounded between $\alpha = -50$ V and $\beta = 50$ V.

TABLE I

MODEL PARAMETERS

Parameter	Value	Parameter	Value
R	75 Ω	m	1.6 g
N	1200	k_s	55 N/m
k_1	$2.7{\cdot}10^{10}$ H^{-1}/m	z_s	15 mm
k_2	$3.25{\cdot}10^{6}$ H^{-1}	c	0 Ns/m
k_3	25 μWb	$[z_{\min}, z_{\max}]$	$[0, 1]$ mm

A. Nominal system

For each of the two operations, five different soft-landing policies have been computed using the nominal model of Section II. These correspond to the time-optimal (TO) solution and four energy-optimal (EO) strategies. The TO policy has been firstly computed to determine the minimum time required by the system to achieve a soft-landing motion. Then, EO solutions have been found for final times equal to 102% (EO_1), 105% (EO_2), 110% (EO_3) and 120% (EO_4) of the TO final time. The results of the simulations are presented in Figs. 3 and 4. For the sake of clarity, these figures only include the TO, EO_2 and EO_4 solutions; the other two are intermediate trajectories. The contact instant using each policy is marked with a dot.

As shown in the figures, the TO policy is of Bang-off-Bang type, i.e., the input switches between α, 0 and β. During the making operation, this strategy increases rapidly the flux to generate a strong force towards zero gap. Then, the magnetic force is decreased to zero until nearly the end of the motion, when it is again increased so that the mover arrives with zero acceleration. On the other hand, the motion during the breaking operation is primarily governed by the elastic force. The initial flux is rapidly decreased to zero so that no magnetic force opposes the motion. Then, at the end of the trajectory, the flux is increased to generate a force that slows down the plunger and makes it reach the final position with zero velocity. As expected, the EO policies are smoother and cause the input to vary continuously on the interval $[\alpha, \beta]$, but this is achieved at the expense of having larger final times. Note that, although there is not a great difference, the asymmetry in the forces causes the two operations to have different optimal-time durations (2.511 ms for making and 2.401 ms for breaking).

The nominal model has been also used for an additional analysis. In this regard, note that the usual non-controlled activation policy with these actuators consists in applying a constant positive voltage in the making operation and another voltage—zero or very close to zero—in the breaking. Hence, we have analyzed how the final time and the impact velocity depend on these voltages. The results are presented in Figs. 5 and 6. As shown, the minimum achievable impact velocity at the end of the making operation is about 0.99 m/s, which corresponds to a voltage of about 16 V and a final time of 4.5 ms. On the other hand, the impact velocity on the breaking operation could be reduced down to 0.76 m/s when using a 2.25 V dc voltage. Lower voltages for the making or higher for the breaking do not produce motion. These values

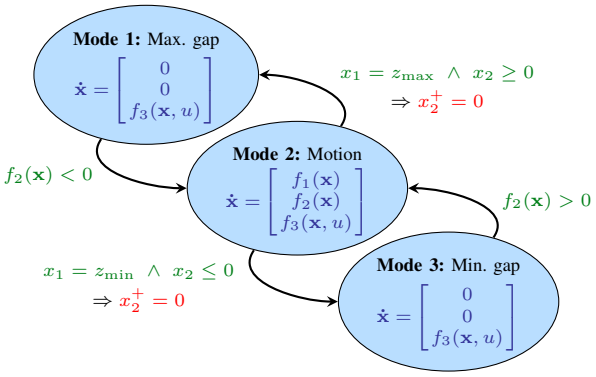

Fig. 2. Hybrid automaton modeling the dynamics of the actuator.

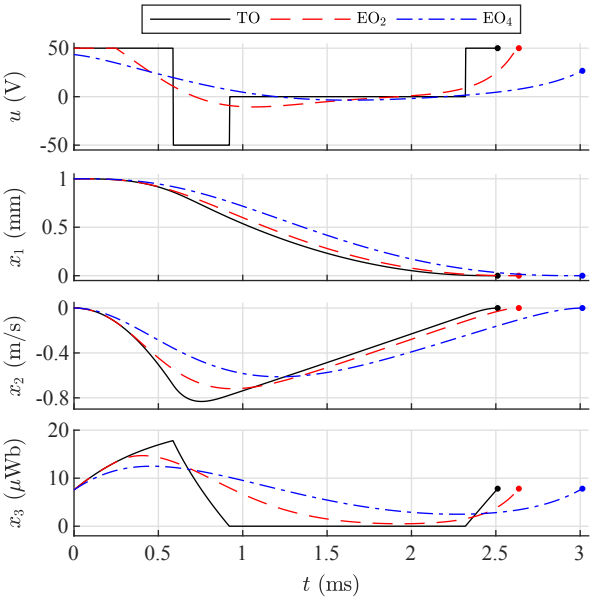

Fig. 3. Optimal soft-landing trajectories for the making operation. From top to bottom: voltage (input), position, velocity and magnetic flux.

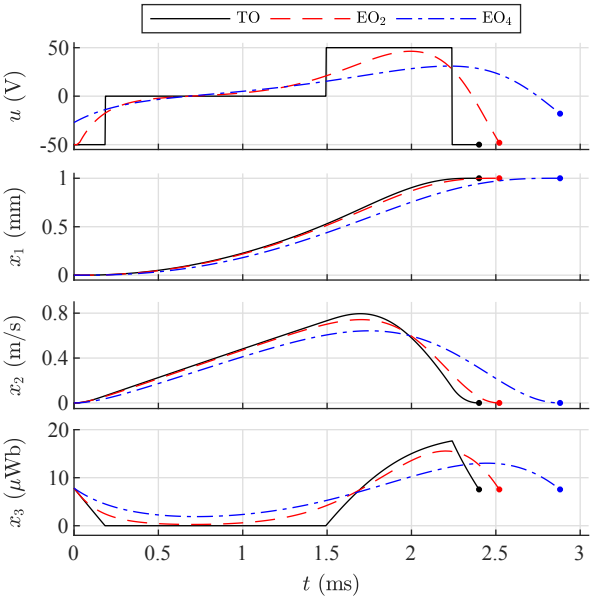

Fig. 4. Optimal soft-landing trajectories for the breaking operation. From top to bottom: voltage (input), position, velocity and magnetic flux.

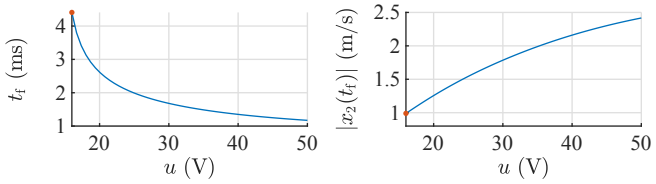

Fig. 5. Final time (left) and absolute value of the impact velocity (right) in non-controlled constant-voltage making operations. The case of minimum impact velocity is marked with a red dot.

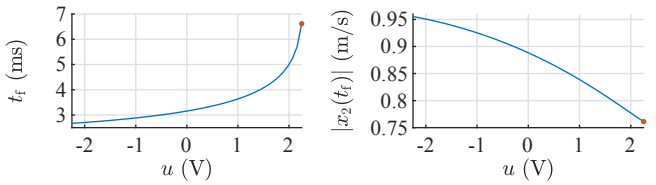

Fig. 6. Final time (left) and absolute value of the impact velocity (right) in non-controlled constant-voltage breaking operations. The case of minimum impact velocity is marked with a red dot.

are used as a benchmark to analyze the performance of the designed optimal control policies on perturbed systems.

B. Perturbed system

As stated in the introduction, the difficulty in measuring or estimating variables and the very high speed of reluctance actuators motivate the search of open-loop soft-landing control policies which can be easily implemented and applied in practice. Considering that the main problem of open-loop control is the lack of robustness against disturbances, in this section we analyze the results of applying the already presented input profiles on perturbed systems.

For that, 25,000 Monte Carlo simulations have been performed for each operation and control policy using the hybrid model in Fig. 2. The nominal parameter vector

$$\mathbf{p} = \begin{bmatrix} R & N & k_1 & k_2 & k_3 & m & k_s & z_s \end{bmatrix}^\mathsf{T} \tag{38}$$

is replaced in the simulations by $\mathbf{p_{pert}}$, which is randomly generated from a normal distribution, $\mathbf{p_{pert}} \sim N(\mathbf{p}, \Sigma^2)$, where $\Sigma = \mathrm{diag}\,(0.01\mathbf{p})$. The value of Σ has been set accordingly to the usual variability of the parameters in commercial actuators. The rest of the parameters remain unchanged. Considering that the mover may bounce at the end of the motion, two different variables are extracted from each simulation. First, the final time, t_{end}, which is not the time of the first impact but the time at which the motion ends. Secondly, an equivalent impact velocity, v_{eq}, calculated as

$$v_{\mathrm{eq}} = +\sqrt{\frac{m_{\mathrm{pert}}}{m} \sum_i \left(x_2(t_i)\right)^2}, \tag{39}$$

where m_{pert} is the perturbed mass and $\{t_i\}$ is the set of time instants at which an impact occurs. This variable represents the velocity that the nominal system should have in order to dissipate on one impact the same amount of kinetic energy than the perturbed system on all the bounces. Since the simulations can take longer than t_f, where t_f is the nominal final time, the input is extended in time using a constant voltage (50 V for making and 0 V for breaking).

The results for the making and breaking operations are respectively presented in Figs. 7 and 8. In both figures, it can be seen that the best values obtained in the simulations are close to those of the nominal case. However, almost all the simulations take longer times and have nonzero values of v_{eq}, which means that soft landing is not perfectly achieved. In any case, it must be noted that the equivalent impact velocities in the great majority of the simulations are smaller than the impact velocities of the non-controlled case (indicated by dash-dot lines in the graphs). In this regard, the mean values are between 45% and 70% smaller than if no control is applied. Therefore, we can conclude that all the proposed policies are advantageous in the search of soft landing with respect to the standard activation.

Focusing on the making operation (see Fig. 7), it can be seen that the best results are undoubtedly those corresponding to the TO policy. The median and mean values, as well as the interquartile range, are clearly better in both the impact velocity and the final time. There is a worsening trend with t_f and, consequently, the worst results are those given by the EO_4 policy. Additionally, the histograms show that the simulations in which there are bounces are slightly worse in both variables, and the effect is similar for the five proposed policies. The bouncing phenomenon is however much more pronounced in the breaking operation (see Fig. 8), what leads to very different results depending on whether there are bounces or not. In this regard, there is not one best policy for this operation with respect to the impact velocity (see, e.g., that the TO policy has the best median value, but it has the worst third quartile). In any case, the minimum mean impact velocity corresponds to the EO_3 policy, whereas the minimum mean final time is obtained with the TO strategy.

V. CONCLUSIONS

In this paper we have presented and compared five different open-loop control policies to achieve soft-landing on a class of nonlinear actuators. Firstly, the dynamic equations of the system have been studied and its main particularities highlighted. The magnetic force, which can only act in one direction, establishes an asymmetry in the motion and has proved to be one of the main control limitations.

Solutions corresponding to the five strategies have been computed for the two possible motions of a nominal actuator. Then, the robustness of applying the open-loop policies on perturbed systems has been analyzed via Monte Carlo simulations. It has been shown that, although soft landing is not completely achieved, the impact velocity is reduced in the great majority of the cases. In this regard, the mean reduction with the best policy in the making operation is about 60%, while in the breaking motion reaches about 70%. These results, together with the simple implementation that the proposed strategies would have in practice, suggest that open-loop optimal control could be a practical and cost-effective approach to achieve soft landing on reluctance actuators.

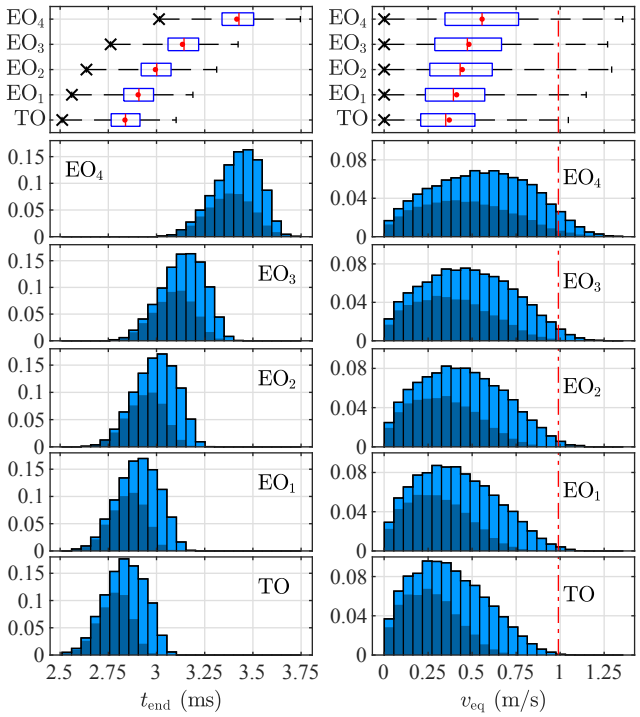

Fig. 7. Box plot and relative frequency histograms of t_{end} (left) and v_{eq} (right) using the open-loop control policies proposed for the making operation. In the box plot, the crosses indicate the values obtained in the nominal case and the dots are the mean values of the distributions. The whiskers extend to the most extreme data points. The dark fraction of the histogram represents the simulations with no bounces. The dash-dot line indicates the lowest possible impact velocity of the non-controlled case.

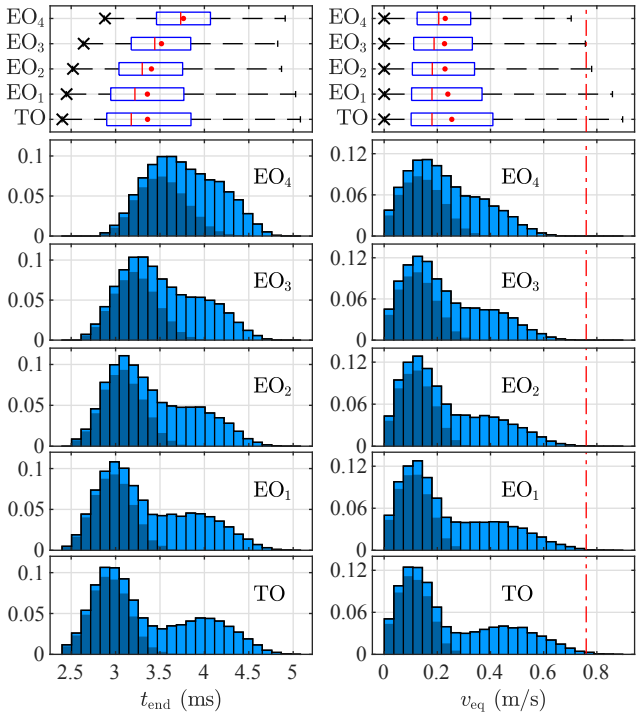

Fig. 8. Box plot and relative frequency histograms of t_{end} (left) and v_{eq} (right) using the open-loop control policies proposed for the breaking operation. In the box plot, the crosses indicate the values obtained in the nominal case and the dots are the mean values of the distributions. The whiskers extend to the most extreme data points. The dark fraction of the histogram represents the simulations with no bounces. The dash-dot line indicates the lowest possible impact velocity of the non-controlled case.

References

[1] A. Katalenic, H. Butler, and P. P. J. van den Bosch, "High-precision force control of short-stroke reluctance actuators with an air gap observer," *IEEE/ASME Trans. Mechatronics*, vol. 21, no. 5, pp. 2431–2439, 2016.

[2] J. Bao, N. H. Vrijsen, B. L. J. Gysen, R. L. J. Sprangers, and E. A. Lomonova, "Optimization of the force density for medium-stroke reluctance actuators," *IEEE Trans. Ind. Appl.*, vol. 50, no. 5, pp. 3194–3202, Sep. 2014.

[3] P. Enrici, F. Dumas, N. Ziegler, and D. Matt, "Design of a high-performance multi-air gap linear actuator for aeronautical applications," *IEEE Trans. Energy Convers.*, vol. 31, no. 3, pp. 896–905, Sep. 2016.

[4] P. Barkan, "A study of the contact bounce phenomenon," *IEEE Trans. Power App. Syst.*, no. 2, pp. 231–240, Feb. 1967.

[5] E. Ramirez-Laboreo, C. Sagues, and S. Llorente, "A new model of electromechanical relays for predicting the motion and electromagnetic dynamics," *IEEE Trans. Ind. Appl.*, vol. 52, no. 3, pp. 2545–2553, May/Jun. 2016.

[6] B. Xu, R. Ding, J. Zhang, L. Sha, and M. Cheng, "Multiphysics-coupled modeling: Simulation of the hydraulic-operating mechanism for a sf6 high-voltage circuit breaker," *IEEE/ASME Trans. Mechatronics*, vol. 21, no. 1, pp. 379–393, Feb. 2016.

[7] E. Ramirez-Laboreo and C. Sagues, "Reluctance actuator characterization via fem simulations and experimental tests," *Mechatronics*, vol. 56, pp. 58 – 66, Dec. 2018.

[8] E. Ramirez-Laboreo, M. G. L. Roes, and C. Sagues, "Hybrid dynamical model for reluctance actuators including saturation, hysteresis and eddy currents," *IEEE Trans. Mechatronics*, in press.

[9] J. R. M. van Dam, B. L. J. Gysen, E. A. Lomonova, and M. Dhaens, "Soft-landing control of low-energy solenoid valve actuators," in *13th Int. Conf. Ecological Vehicles and Renewable Energies*, Apr. 2018, pp. 1–5.

[10] J.-H. Lee, Y.-W. Yun, H.-W. Hong, and M.-K. Park, "Control of spool position of on/off solenoid operated hydraulic valve by sliding-mode controller," *J. Mech. Sci. Technol.*, vol. 29, no. 12, pp. 5395–5408, Dec. 2015.

[11] E. Moya-Lasheras, C. Sagues, E. Ramirez-Laboreo, and S. Llorente, "Nonlinear bounded state estimation for sensorless control of an electromagnetic device," in *IEEE Conf. Decision and Control*. IEEE, Dec. 2017, pp. 5050–5055.

[12] T. Braun, J. Reuter, and J. Rudolph, "Observer design for self-sensing of solenoid actuators with application to soft landing," *IEEE Trans. Control Syst. Technol.*, 2018.

[13] N. H. Vrijsen, J. W. Jansen, and E. A. Lomonova, "Prediction of magnetic hysteresis in the force of a prebiased e-core reluctance actuator," *IEEE Trans. Ind. Appl.*, vol. 50, no. 4, pp. 2476–2484, Jul. 2014.

[14] M. Benosman and G. M. Atınç, "Extremum seeking-based adaptive control for electromagnetic actuators," *Int. J. Control*, vol. 88, no. 3, pp. 517–530, 2015.

[15] J. Tsai, C. R. Koch, and M. Saif, "Cycle adaptive feedforward approach controllers for an electromagnetic valve actuator," *IEEE Trans. Control Syst. Technol.*, vol. 20, no. 3, pp. 738–746, May 2012.

[16] E. Ramirez-Laboreo, C. Sagues, and S. Llorente, "A new run-to-run approach for reducing contact bounce in electromagnetic switches," *IEEE Trans. Ind. Electron.*, vol. 64, no. 1, pp. 535–543, Jan. 2017.

[17] S. K. Chung, C. R. Koch, and A. F. Lynch, "Flatness-based feedback control of an automotive solenoid valve," *IEEE Trans. Control Syst. Technol.*, vol. 15, no. 2, pp. 394–401, Mar. 2007.

[18] T. Glück, W. Kemmetmüller, and A. Kugi, "Trajectory optimization for soft landing of fast-switching electromagnetic valves," *IFAC Proc. Vol.*, vol. 44, no. 1, pp. 11 532–11 537, Jan. 2011.

[19] A. Fabbrini, A. Garulli, and P. Mercorelli, "A trajectory generation algorithm for optimal consumption in electromagnetic actuators," *IEEE Trans. Control Syst. Technol.*, vol. 20, no. 4, pp. 1025–1032, Jul. 2012.

[20] J. J. Cathey, *Electric machines: analysis and design applying Matlab*. McGraw-Hill, 2001.

[21] S. D. Sudhoff, *Power magnetic devices: a multi-objective design approach*. John Wiley & Sons, 2014.

[22] D. S. Naidu, *Optimal Control Systems*, 1st ed., ser. Electrical Engineering Series. CRC Press, 2002.

[23] D. E. Kirk, *Optimal Control Theory - An Introduction*. Dover Publications, 1998.